Atmos. Chem. Phys. Discuss., https://doi.org/10.5194/acp-2019-81
Manuscript under review for journal Atmos. Chem. Phys.
Discussion started: 1 March 2019


Atmospheric Chemistry and Physics Discussions
Open Access

# The impact of increases in South Asian anthropogenic emissions of $SO_2$ on sulfate loading in the upper troposphere and lower stratosphere during the monsoon season and the associated radiative impact

Suvarna Fadnavis[1], Gayatry Kalita[1], Matthew Rowlinson[2], Alexandru Rap[2], Jui-Lin Frank Li[3], Blaž Gasparini[4] Anton Laakso[5] and Rolf Müller[6]

[1]Indian Institute of Tropical meteorology, Pune, India

[2]School of Earth and Environment, University of Leeds, Leeds, UK.

[3]Jet Propulsion Laboratory, California Institute of Technology, Pasadena, California, USA

[4]Department of Atmospheric Sciences, University of Washington, Seattle, USA

[5]Finnish Meteorological Institute, Finland

[6]Forschungszentrum Jülich GmbH, IEK7, Jülich, Germany

Corresponding authors: suvarna@tropmet.res.in

Abstract:

The Asian summer monsoon plays a key role in changing aerosol amounts in the upper troposphere and lower stratosphere (UTLS) via convective transport. Here, we use the ECHAM6–HAMMOZ global chemistry–climate model to investigate the transport of anthropogenic South Asian sulfate aerosols and their impact on the UTLS. Our experiments (ten-member ensemble) with $SO_2$ emissions enhanced by 48 % over South Asia, based on an

Atmos. Chem. Phys. Discuss., https://doi.org/10.5194/acp-2019-81
Manuscript under review for journal Atmos. Chem. Phys.
Discussion started: 1 March 2019


Ozone Monitoring Instrument (OMI) satellite observed rising trend of ~4.8 % per year during 2006 – 2017, simulate how the Asian sulfate aerosols are convectively transported to the UTLS. The tropospheric increase in $SO_2$ leads to an increase in UTLS sulfate aerosol loading of 10 – 33 % over South Asia and 5 – 10 % over the high latitudes in the northern hemisphere. The enhanced sulfate aerosols lead to warming (0.1±0.06 to 0.6±0.25 K) in the lowermost stratosphere and cooling (-0.1±0.06 to -0.8±0.41 K) in the troposphere in the Northern Hemisphere. The estimated mean direct radiative forcing at the top of the atmosphere (TOA) induced by the increase in South Asian aerosol emissions is -0.2 to -1.5 $W{\bullet}m^{-2}$over north India during the monsoon season. The decrease in vertical velocity and the associated enhanced stability of the upper troposphere in response to increased $SO_2$ emissions will likely have a weakening effect on the South Asian monsoon.

Key words: sulfate aerosols, radiative forcing, upper troposphere and lower stratosphere, South Asia.

Atmos. Chem. Phys. Discuss., https://doi.org/10.5194/acp-2019-81
Manuscript under review for journal Atmos. Chem. Phys.
Discussion started: 1 March 2019


## 1. Introduction

Understanding the effects of rapid increases in anthropogenic sulfur dioxide ($SO_2$) emissions in South Asia is very important both for air quality, as they lead to haze formation and significant human health and crop yield impacts (Li et al., 2017), and for climate and the hydrological cycle (Guo et al., 2016). Sulfur dioxide is converted into sulfuric acid, which forms sulfuric acid-water particles (aerosol particles), which scatter and absorb solar and infrared radiation (direct radiative forcing), causing cooling at the surface and warming the atmosphere locally (Niemeier and Schmidt, 2017). A variety of aerosol particles including sulfate aerosol particles are important for ice cloud formation in the atmosphere (DeMott et al., 2010); sulfate aerosols also act as condensation nuclei in cloud formation processes, increasing cloud albedo and changing cloud microphysical properties (indirect radiative forcing) (Smith et al., 2011).

The sustained economic growth in India during the last few decades has been driving a large rising trend in emissions of $SO_2$. Satellite observations show ~50 % increase in $SO_2$ emission over South Asia during the past decade (Krotkov et al., 2016). According to the 1999 Indian Ocean Experiment (INDOEX), sulfate aerosols are responsible for 29 % of the observed aerosol optical depth (AOD) over the Indian region (Verma et al., 2012).The Network of aerosol observatories established under the Aerosol Radiative Forcing (ARFINET) measurements over India show a consistent rising annual trend in AOD of 0.004 during 1988 – 2013 (Babu et al., 2013). All these rising trends point to an increase in aerosol impacts, with potentially important climatic effects (e.g. increased radiative forcing, changes in monsoon precipitation) (Ramanathan et al., 2005; Guo et al., 2016).

The current best estimate of global sulfate aerosol direct radiative forcing (RF) is -0.4 W•m$^{-2}$ (-0.6 W•m$^{-2}$ to -0.2 W•m$^{-2}$) (Myhre et al., 2013). The INDOEX experiment (January to March 1999) recorded a sulfate aerosol AOD range of 0.1 – 0.14, and a regional direct radiative forcing of -1.25 to -2.0 W•m$^{-2}$ at TOA over North India (Verma et al., 2012). The variability of sulfate aerosols over the Indian region and their associated radiative forcing in the context of convective transport to the upper troposphere and lower stratosphere (UTLS) is not well understood. A number of studies reported linkages of rising trends in AOD with observed decreasing trends in Indian summer monsoon rainfall via changes in radiative forcing, surface cooling and a decreasing land–ocean temperature gradient (Ramanathan et al., 2005). A decrease in monsoon precipitation over South Asia can potentially affect the south Asian region economy, agriculture as well as the life of billions of people (~80 % of annual rainfall is received during June and September) (Paul et al., 2016). It is therefore important to understand the impact of the observed rising trends in Asian $SO_2$ emissions over the south Asian region on radiative forcing and the associated effects.

Recent satellite observations show a layer of aerosols in the upper troposphere and lower stratosphere (UTLS) known as the Asian Tropopause Aerosols Layer (ATAL) (Vernier et al., 2011; 2015). The formation and maintenance of the ATAL is linked to the convective pumping of aerosols and aerosol precursors into the UTLS by the Asian summer Monsoon (Fadnavis et al., 2013; Vernier et al., 2015; Yu et al., 2017). While the majority (~80 %) of sulfur emissions from South Asia is removed by precipitation, the remaining fraction is transported into the uppermost troposphere and lower stratosphere contributing to the ATAL (associated with the monsoon anticyclone). Two thirds of the total aerosols loading that reach the monsoon anticyclone are transported pole ward through circulation in the lower stratosphere (Lelieveld et al., 2018). The observed $SO_2$ concentrations in the monsoon anticyclone are ~5 – 10 times higher than throughout the rest of the tropics (Lelieveld et al., 2018). The major sources of aerosols in the ATAL are found in South Asia and East Asia with South Asian emissions dominating the composition of the ATAL (Lau et al., 2018). Since 2005, sulfur emissions over China show a decrease of about 50 % (Krotkov et al., 2016), while they continued to increase over South Asia (Li et al., 2017). This indicates that sulfur emitted from South Asia may in the near future contribute substantially to the composition of the ATAL. Climate model simulations show that the Asian region is three times more efficient (per unit area and time) in enhancing aerosol in the Northern Hemisphere stratosphere than tropical upwelling (Yu et al., 2017). Although the chemical composition of the particles constituting the ATAL is not well understood, satellite observations (e.g. Cloud–Aerosol Lidar and Infrared Pathfinder Satellite Observation (CALIPSO), Stratospheric Aerosol and Gas Experiment (SAGE–II)), balloonsonde and aircraft measurements (e.g. Civil Aircraft for the Regular Investigation of the atmosphere Based on an Instrumented Container (CARIBIC)) suggest that ATAL particles contain large amounts of sulfate, as well as black carbon, organic, nitrates and dust (Vernier et al., 2011; 2018; Yu et al., 2015; 2016). Further, model studies suggest sulfate, together with organics, as a major chemical component of the ATAL (e.g., Fadnavis et al., 2013; Yu et al., 2015). However, there is also a model study (Gu et al., 2016) that emphasizes the importance of nitrate as a chemical component of the aerosol in the UTLS over the Tibetan Plateau and the South Asian summer monsoon region. And balloon measurements made from Hyderabad, India show the presence of large amounts of nitrate aerosols near the tropopause (100 ng $m^{-3}$), which may be due to $NO_X$ from anthropogenic emissions, lightning, and gas-to-aerosol conversion (Vernier et al., 2018). Vernier et al. (2011, 2015, 2018) and Yu et al. (2015, 2016, 2017) report that sulfate and nitrate aerosols are important components of the ATAL. The increasing Asian $SO_2$ emissions are a focus of many studies due to their impacts on a decrease in summer monsoon precipitation (Kim et al., 2016; Meehl et al., 2004; 2000). The reinforcement of the monsoon circulation and the associated changes in monsoon precipitation results from radiative cooling by the sulfate aerosol forcing. Aerosol loadings in the UTLS result in a significant impact on radiative forcing for example, satellite observations show that the ATAL layer has exerted a regional radiative forcing at the top of the atmosphere of approximately -0.1 W•m$^{-2}$ in the past 18 years, thus locally reducing the impact of global warming (Vernier et al., 2015).

In this study, we investigate the impacts of rising South Asian $SO_2$ emissions when distributed globally by the monsoon convection, using the state of art aerosol-chemistry-climate model ECHAM6–HAMMOZ (version echam6.1.0-ham2.1-moz0.8). The key questions we address here are: (1) what is the contribution of increased $SO_2$ emissions from South Asia to the ATAL? (2) What is the associated radiative forcing? (3) Can the increase in South Asian $SO_2$ emissions change the dynamics and clouds in the UTLS?

The paper is organized as follows: Section 2 describes the model and satellite data. A short model evaluation follows in Section 3. The distribution of aerosols in the UTLS is discussed in Section 4. The impact of sulfate aerosols on radiative forcing, heating rates, cloud ice, and temperature are presented in Section 5. Finally, section 6 presents the conclusions of this study.

## 2. Measurements and model simulations

### 2.1 Satellite and ground bases measurements of AOD

We analyze aerosol retrievals from multiple satellites e.g. Multi-Angle Imaging Spectroradiometer (MISR) (level-3 version 4, at 550 mn wavelength during 2000 – 2016) (Martonchik et al., 2002), Total Ozone Mapping Spectrometer (TOMS) Earth probe aerosol index (AI) (level-3, during 1997 – 2005) (McPeters et al., 1996). The MISR AOD measurements give aerosol properties over the global ocean and land with bright targets such as deserts (Kahn et al. 2001). The spatial distribution of MISR and TOMS measurements are consistent over most of the regions (Zhang and Christopher 2003). Aerosol-Robotic-NETwork (AERONET) sun photometer, level 2.0 version 3 daily AOD observations during 2006 – 2016 (Holben et al., 1998) were also analyzed at four stations over the Indo–Gangetic Plain, Bihar (84.12 °E , 25.87 °N), Jaipur (75.80 °E, 26.90 °N), Kanpur (80.23 °N, 26.51 °N), Karachi (67.13 °N, 24.95 °N).

### 2.2 $SO_2$ measurements from Ozone Monitoring Instrument (OMI)

The Ozone Monitoring Instrument (OMI) aboard the NASA Aura spacecraft retrieves $SO_2$ data from Earthshine radiances in the wavelength range of 310.5 – 340 nm (Levelt, et al., 2006). It gives the total number of $SO_2$ molecules in the entire atmospheric column above a unit area (https://disc.gsfc.nasa.gov/datasets/OMSO2e_V003/). Details of the retrieval technique are documented by Li et al., (2013, 2017). $SO_2$ emissions over China have recorded a decreasing trend since 2006 (Krotkov et al., 2016) while in South Asia they continued to rise (Li et al., 2017). In order to understand the impact of increasing South Asian $SO_2$ emissions we estimate a trend in $SO_2$ burden (2007 – 2017) over the Indian region (70 – 95 °E, 8 – 35

°N, see Fig. 1c). For this purpose, we used version 1.3, level-2, OMI retrievals that assume all $SO_2$ is located in the planetary boundary layer. We use a regression model described by Fadnavis et al., (2014) and Fadnavis and Beig (2006). A model regression equation is given as follows:

$$\theta(t,z) = \alpha(z) + \beta(z)\ \mathrm{Dayindex}\ (t) \qquad \mathbf{(1)}$$

where $\theta(t,z)$ is the daily mean number of $SO_2$ molecules averaged over the Indian region, with altitude z set to 1 km, as we use column data. The model uses the harmonic expansion to calculate the seasonal coefficient, $\alpha$, and the trend coefficient, $\beta$. The harmonic expansion for $\alpha(t)$ is given as:

$$\alpha(t) = A_0 + A_1 \cos \omega t + A_2 \sin\omega t + A_3 \cos 2\omega t + A_4 \sin 2\omega t \qquad \mathbf{(2)}$$

Where$\omega = 2\pi/12$; A0, $A_1$, $A_2$ ……. are constants and t (t=1,2 ….n) is the time index. The estimated trend value is 4.8 ± 0.97 % $yr^{-1}$. This trend value is used while designing the model sensitivity experiments (discussed in section 2.4).

### 2.3 CloudSat and Cloud-Aerosol Lidar Infrared Pathfinder Satellite Observations (CALIPSO)

We use the ice water content (IWC) dataset from a combination of CALIPSO lidar and CloudSat radar data (2C–ICE dataset, version L3_V01) for the period 2007 – 2010 (Deng et al., 2013). The Cloud Profiling Radar (CPR) onboard the CloudSat satellite is a 94 GHz nadir-looking radar which measures the power backscattered by clouds as a function of distance. It provides information on cloud abundance, distribution, structure, and radiative properties. The Cloud-Aerosol Lidar with Orthogonal Polarization (CALIOP) is an elastically backscattered

Atmos. Chem. Phys. Discuss., https://doi.org/10.5194/acp-2019-81
Manuscript under review for journal Atmos. Chem. Phys.
Discussion started: 1 March 2019


active polarization-sensitive lidar instrument onboard CALIPSO. CALIOP transmits laser light simultaneously at 532 and 1064 nm at a pulse repetition rate 20.16 Hz. The lidar receiver subsystem measures backscatter intensity at 1064 nm and two orthogonally polarized components of 532 nm backscatter signal that provide the information on the vertical distribution of aerosols and clouds, cloud particle phase, and classification of aerosol size (Winker et al., 2010). The details of the data retrieval method are explained in Li et al. (2012).

### 2.4 The model simulations

The ECHAM6–HAMMOZ aerosol–chemistry–climate model (Schulz et al., 2018) used in the present study comprises of the ECHAM6 global climate model (Stevens et al., 2013) coupled to the two moment aerosol and cloud microphysics module HAM (Stier et al., 2005; Zhang et al., 2012; Tegen et al., 2018) and the sub-model for trace gas chemistry MOZ (Kinnison et al., 2007). HAM predicts the nucleation, growth, evolution, and sinks of sulfate ($SO_4^{2-}$), black carbon (BC), particulate organic matter (POM), sea salt (SS), and mineral dust (DU) aerosols. The size distribution of the aerosol population is described by seven log-normal modes with prescribed variance as in the M7 aerosol module (Vignati et al., 2004; Stier et al., 2005; Zhang et al., 2012). Moreover, HAM explicitly simulates the impact of aerosol species on cloud droplet and ice crystal formation. Aerosol particles can act as cloud condensation nuclei or ice nucleating particles. Other relevant cloud microphysical processes such as evaporation of cloud droplets, sublimation of ice crystals, ice crystal sedimentation, detrainment of ice crystals from convective cloud tops, etc. are simulated interactively (Lohmann et al., 2010; Neubauer et al., 2014). The anthropogenic and fire emissions of sulfate, BC, and OC are based on the AEROCOM-ACCMIP-II emission inventory (Textor et al., 2006). (The distribution of the sulfate emission mass flux ($kg{\bullet}m^{-2}{\bullet}s^{-1}$) averaged for June–

Atmos. Chem. Phys. Discuss., https://doi.org/10.5194/acp-2019-81
Manuscript under review for journal Atmos. Chem. Phys.
Discussion started: 1 March 2019


September show high amounts over South Asia (see Fig. S1). The MOZ sub-model describes the trace gas chemistry from the troposphere through to the lower thermosphere. The species included within the chemical mechanism are contained within the OX, $NO_X$, $HO_X$, $ClO_X$, and $BrO_X$ chemical families, along with $CH_4$ and its degradation products. Several primary non-methane hydrocarbons (NMHCs) and related oxygenated organic compounds are also included. This mechanism contains 108 species, 71 photolytic processes, 218 gas-phase reactions, and 18 heterogeneous reactions on aerosol (Kinnison et al., 2007). Details of anthropogenic, biomass burning, biogenic, emissions fossil fuel sources etc. are reported by Fadnavis et al. (2017a).

The model simulations are performed at the T63 spectral resolution corresponding to 1.875°× 1.875° in the horizontal dimension, while the vertical resolution is described by 47 hybrid σ-p levels from the surface up to 0.01 hPa. The simulations have been carried out at a time step of 20 minutes. AMIP (add reference) sea surface temperature (SST) and sea ice cover (SIC) were used as lower boundary conditions. We performed 10-member ensemble runs by varying the initial conditions (both SST and SIC) starting between 1 and 10 January 2010 and ending at 31 December 2011 to obtain statistical significant results. The analysis is performed for the year 2011. The 2011 Indian monsoon was relatively normal, with no strong influences from the Indian Ocean Dipole or El Niño modes of inter-annual climatic variability. We refer to it as the control simulation (CTRL). In previous work, Fadnavis et al. (2013; 2017c) used the ensemble means from 6–10 members to analyze the variability of aerosols and associated impacts during the monsoon season. In the emission sensitivity simulations (referred to as Ind48), we have applied a flat 48% increase in anthropogenic $SO_2$ emissions over India (8 – 40 °N, 75 – 95 °E) (same for all the years), based on the estimated trend of 4.8

% per year in OMI $SO_2$ observations during 2007 – 2017. The Ind48 simulations are also 10 member ensemble runs for the same period as CTRL and analyzed for the year 2011 (See Table-1). We compare the CTRL and Ind48 simulations in order to understand the impact of enhanced sulfate aerosol on the UTLS, radiative balance, and cirrus clouds during the monsoon season.

We must mention that our experiments are necessarily canonical in design to show the impact of Asian sulfate aerosols; they do not include many of the observed complexities, like radiative forcing due to non-sulfate aerosols (e.g. organics, nitrates, and dust etc.). Notwithstanding this, this work provides valuable insight into the relevance of the impact of sulfate aerosol originating from south Asia on the UTLS, where $SO_2$ emissions show continued increase while $SO_2$ emissions are declining over East Asia.

### 2.5 Offline radiative calculations

We use offline radiative calculations to explore the radiative impacts of enhanced sulfate aerosol loadings in the UTLS only (300 – 50 hPa), compared to the all atmosphere enhancement. Heating rates and radiative effects associated with the sulfate aerosol enhancement are calculated using the SOCRATES radiative transfer model (Edwards and Slingo, 1996; Rap et al., 2013) with the CLASSIC aerosol scheme (Bellouin et al., 2011). We used the offline version of the model with six shortwave and nine longwave bands, and a delta-Eddington two-stream scattering solver at all wavelengths.

## 3. Model evaluation with satellite observation

In Fig. 1a–b we show the distribution of cloud ice from ECHAM6–HAMMOZ and combined measurements of total cloud ice from CloudSat and CALIPSO (2C–ICE) (2007 –

2010). Both the model simulations (8 – 18 mg•kg$^{-1}$) and observations (8 – 20 mg•kg$^{-1}$) show high amounts of cloud ice in the mid-upper troposphere (450 – 250 hPa) over the Asian monsoon region. The distributions of simulated cloud ice show a maximum over South Asia while the CloudSat and CALIPSO observations indicate maxima over Asia (70 – 120°E). The differences in model simulations and observations may be related to uncertainties in satellite observations and model biases (Li et al., 2012); for example, the model does not consider large ice particles unlike the cloud ice measurement from CloudSat and CALIPSO. The total ice water mass estimates from 2C–ICE combine measurements from CALIPSO lidar depolarization, which is sensitive to small ice particles (i.e., cloud ice represented in global climate models), and CloudSat radar, which is very sensitive to larger ice particles (i.e., precipitating ice or snow) (Li et al., 2012).

Figure 1c-e shows the distribution of seasonal mean AOD from MISR (2000 – 2016), model simulations and AERONET observations (2006 – 2016) (Bihar, Jaipur, Kanpur, Karachi) over the Indo–Gangetic Plain. TOMS aerosol index (1997 – 2005) is shown in Fig 1f. MISR and TOMS indicates high amounts of aerosols over the Indo–Gangetic Plains and northern Arabian Sea. The magnitude of simulated AOD is in agreement with MISR over the Indo-Gangetic plain (~0.4 – 0.5) and over west Asia the model shows an underestimation by ~0.35. Comparison with AERONET observations shows that simulated AOD is underestimated over the Indo-Gangetic plain (0.23 – 0.35). The differences in magnitude of AOD between model, satellite remote sensing (MISR) and AERONET observations may be due to various reasons for e.g. underestimation of dust aerosols in the model (Kokkola et al., 2018). Satellite remote sensing detects AOD from top of the atmosphere while AERONET detects AOD from the ground. In AERONET, aerosols above 4 km contribute 50 % of AOD

(Dumka et al. 2014). Inclusion of nitrate aerosol may affect the distribution of the AOD. During the monsoon season, dust is transported from west Asia to the Arabian Sea via the low level monsoon jet (Vinoj et al., 2014). Distribution of TOMS AI which is sensitive to absorbing aerosols (like dust particles) also show high magnitude over Arabian Sea and West Asia. In the past, largest differences between annual mean AOD (0.23 – 0.3) over South Asia and Southeast Asia between the ECHAM6–HAMMOZ model and observations (MODIS) are reported by Kokkola et al., (2018). Majority of CMIP5 models underestimate global mean dust optical depth (Pu and Ginoux, 2018). There are uncertainties in model estimates of sea salt emission and parameterization too (Spada et al., 2013). High magnitude of AOD near 25 °N, 75 °E may be due to high amount of sea salt and water soluble aerosols in the model.

## 4. Results

### 4.1 A layer of aerosol in the UTLS

The South Asian region frequently experiences convective instability during pre-monsoon (March–May) and monsoon (June–September) and post-monsoon season (October–November) (Manohar et al., 1999). Convection plays an important role in lifting the boundary layer pollutants to the UTLS (Fadnavis et al., 2013, 2014, 2015). The uplifted aerosols contribute to the formation of a layer over South Asia between April and October (Lau et al., 2018). Convective transport during pre-monsoon and post-monsoon seasons is most by cyclones and thunderstorm (Manohar et al., 1999). The large scale organized convection and the upper level anticyclone during the monsoon season play key roles in formation of Asian Tropopause Aerosols Layer (ATAL) in the UTLS. The CALIPSO lidar and Stratospheric

Aerosol and Gas Experiment II (SAGE-II) satellite observations show ATAL during the monsoon season extending over a wider Asian region (15 – 40 °N, 60 – 120 °E) (Vernier et al., 2011; Fadnavis 2013, 2015).

Both aerosol extinction and sulfate aerosol concentrations from the CTRL simulations show a peak in the UTLS over North India (75 – 95 °E, 25 – 40 °N) from the pre-monsoon to post-monsoon season (April–October) (Fig.2a–b). The sulfate aerosol layer in the UTLS is connected to the troposphere during the pre-monsoon and post-monsoon periods (Fig. 2b), indicating transport of tropospheric sulfate aerosol into the UTLS during these seasons. Strong uplift during the monsoon season lifts the mid-tropospheric aerosols and aerosol precursors to the UTLS generating aerosol minima in the mid troposphere (Fadnavis et al., 2013).

The estimated ratio of ECHAM6–HAMMOZ simulated sulfate aerosols in the ATAL to the total aerosol amount is 6:10 pointing at sulfate aerosols as a major ATAL constituent. Balloonsonde observations over South Asia also show large amounts of sulfate aerosols in the ATAL (Vernier et al., 2015). Although the layer of sulfate aerosols persists throughout the pre-monsoon and monsoon season, in this paper we restrict our analysis to the monsoon season only; this is because large scale convective transport during monsoon season leads to a stronger transport of boundary layer pollutants to the UTLS (Randel et al., 2006; Fadnavis et al., 2015).

The convective transport mostly occurs from the Bay of Bengal and southern slopes of Himalayas (Fadnavis et al., 2013, 2015). Park et al. (2009) have shown that monsoon convection lifts the Asian pollutants into the upper troposphere (~200 hPa) which are then transported north-westward and upward into the anticyclone (Fig.14 therein). After the convective uplift, at altitudes above ~360 K, radiatively driven upward transport in the anticyclonic monsoon circulation occurs at a rate of ~1 K•day$^{-1}$; this is a slower uplift than convection but faster than outside the anticyclone (Vogel et al., 2018). We show the simulated horizontal distribution of aerosol extinction and sulfate aerosols at 100 hPa in the CTRL experiment in Figs. 2c-d. This result indicates maxima in aerosols extinction (Fig. 2c) and sulfate aerosols (Fig. 2d) in the anticyclone region.

### 4.2 Transport into the upper troposphere and lower stratosphere

The climate model simulations and satellite observations show three pathways for convectively lifted aerosols: (i) quasi-isentropic transport from the monsoon anticyclone into the extra-tropical lowermost stratosphere, (ii) cross-isentropic transport from the UTLS into the tropical stratosphere by slow, radiatively driven ascent, and (iii) transport of air into the stratosphere by overshooting convection that sometimes crosses the tropopause in the tropics (Kremser et al., 2016). In order to understand the transport pathways of sulfate aerosol, we analyze anomalies of sulfate aerosols between the simulation with increased sulfate emissions (Ind48) and the control simulation (CTRL, Fig. 3a–b).The distribution of sulfate aerosols show a plume rising from boundary layer into the UTLS occurring through a conduit (from the Indo Gangenic plain and Bay of Bengal region: 15 – 35 °N, 75 – 95 °E). Sulfate aerosol enhancement (~5 – 10 ng•m$^{-3}$) (10 – 33 %) is observed near the tropopause over the Indian region. Cross tropopause transport (2 – 10 ng•m$^{-3}$) is also evident in Fig. 3a-b. In the lowermost stratosphere (100 – 70 hPa), the anomalies of sulfate aerosol extend up to the North Pole (2 – 5 ng•m$^{-3}$) (5 – 10 %) (Fig. 3a) due to the quasi-isentropic transport by the shallow branch of Brewer Dobson circulation (between 380 – 430 K) (Vogel et al., 2014; Rolf et al., 2018). Yu et al., (2017) report that ∼15 % of the Northern Hemisphere column stratospheric aerosol surface area originates from the Asian summer monsoon anticyclone region. Figure 3b shows that aerosols spread to east and west from the anticyclone (20 – 120 °E), likely due to east/westward eddy shedding from the anticyclone (Vogel et al., 2016; Fadnavis and Chattopadhyay, 2017b; Fadnavis et al., 2018). Eddy shedding may not be evident in seasonal mean distribution (Fig. 3 b) since it occurs on a daily scale.

## 5. Impact of enhanced anthropogenic South Asian $SO_2$ emissions

### 5.1 Radiative forcing and heating rates

The net radiative forcing at the TOA (Fig. 4a) and surface (Fig. 4b) due to sulfate aerosols, simulated in our ECHAM6–HAMMOZ experiments is varying between -0.2 and -1.5 $W{\bullet}m^{-2}$ over South Asia and is approximately -0.6 $W{\bullet}m^{-2}$ over the North India (regional mean over 23 – 30 °N, 75 – 85 °E, as shown by the box in Fig. 4a). The positive forcing (both at TOA and surface) simulated over the Arabian Sea may be related to the low values of clouds (Fig. 7a, discussed later in section 5.3) which might very well be caused by anomalies in dust aerosols that certainly interact with cloud formation processes. A positive anomaly in dust aerosol distribution (see Fig.S2) is likely be caused by the dynamical changes induced by the sulfate aerosol enhancement. The transport of dust aerosols from West Asia to the Arabian Sea occurs during the monsoon season (Vinoj et al., 2014). The strong scattering properties of the sulfate aerosols lead to similar TOA and surface forcing (Forster et al., 2007). The negative forcing in the northern hemisphere (0 – 80 °N) (-0.1$W{\bullet}m^{-2}$ in high latitudes) is likely due to the poleward transport of south Asian sulfate aerosols in the lower stratosphere (see Fig. 3a).

Atmos. Chem. Phys. Discuss., https://doi.org/10.5194/acp-2019-81
Manuscript under review for journal Atmos. Chem. Phys.
Discussion started: 1 March 2019


The corresponding TOA sulfate aerosol direct radiative forcing estimated with our offline simulations is shown in Fig 5a. It shows RF varying between - 0.3 to - 2.3 W•m$^{-2}$ over the South Asian region. Over North India estimated RF is ~ -1.38 W•m$^{-2}$ and over mid-high latitudes ~ -0.1 W•m$^{-2}$. These values are lower than the results of the ECHAM6–HAMMOZ simulations. The differences in estimated RF from the offline calculations and the ECHAM6–HAMMOZ simulations are likely due to the fact that the implicit dynamical responses are not captured in the offline experiments. Figure 5b shows the TOA direct radiative forcing (estimated from our offline simulations) induced by the sulfate enhancement in the UTLS (300 – 50 hPa). The RF values vary between ~ -0.012 and -0.02 W•m$^{-2}$ in the anticyclone region (20 – 45 °N, 60 – 120 °E) with a minimum (-0.02 W•m$^{-2}$) at the eastern part of anticyclone (20– 30 °N, 65 – 90 °E). This is collocated with a maximum in sulfate aerosols in the UTLS (Fig. 3). The short term ATAL RF at the top of the atmosphere has been estimated to ~-0.1 W•m$^{-2}$ over the Asian region during 1998 – 2015 (Vernier et al., 2015).

The RF at the TOA obtained from ECHAM6–HAMMOZ simulations (Fig. 4a) is comparable with the INDOEX experiment values corresponding to January – March 1999, i.e. -1.25 to -2.0 W•m$^{-2}$ over North India (Verma et al., 2012). Yu et al. (2016) have reported that the increase in sulfate AOD (0.06 – 0.15) over the tropics (30 °S – 30 °N) since the pre-industrial period has exerted a forcing of -0.6 to -1.3 W•m$^{-2}$.

Figure 6a shows the vertical cross sections of heating rates changes induced by the sulfate enhancement as estimated from the offline radiative transfer model. It shows negative anomalies in the troposphere in northern hemisphere (-0.5 ×10$^{-3}$ K•day$^{-1}$ to -1 ×10$^{-3}$ K•day$^{-1}$) and a large magnitude over south Asia (-1×10$^{-3}$ K•day$^{-1}$). In the UTLS (300 – 50 hPa) heating rate changes due to sulfate aerosols are positive (0.1×10$^{-3}$ K•day$^{-1}$ – 0.9×10$^{-3}$ K•day$^{-1}$) in the northern hemisphere with a maximum over south Asia (10 – 40 °N). The region of positive heating rates coincides with region of positive sulfate aerosol anomalies. This heating is due to absorption of infrared radiation by the stratospheric sulfate aerosols (Heckendorn et al., 2009).

### 5.2 Incoming solar radiation, temperature and stability of the troposphere

One of the impacts of sulfate aerosols in the atmosphere is solar dimming which counteracts part of the temperature response to $CO_2$ increase (Ramanathan et al., 2005). There is observational evidence (1300 sites spread globally) indicating that one third of potential continental warming attributable to increased greenhouse gas concentrations has been compensated by aerosol cooling during 1964 – 2010 (Storelvmo et al., 2016). Solar radiation measurements over the Indian region (at 12 stations) during 1981 – 2004 show a declining trend varying between -0.17 to -1.44 W•m$^{-2}$ year$^{-1}$ (PadmaKumari et al., 2007). Ramanathan et al. (2005) reported a negative trend in solar flux observations at 10 different Indian stations (-0.42 W•m$^{-2}$) and their model simulations show a trend of -0.37 W•m$^{-2}$ induced by the BC and sulfate aerosols over India (0 – 30 °N and 60 – 100 °E).We estimate the changes in net solar radiation at the surface in response to enhanced $SO_2$ emissions. Figure 6b shows negative anomalies of -1 to -3 W•m$^{-2}$ corresponding to a reduction in incoming solar radiation over the Indian region (except over west India: 68 – 77 °E, 17 – 28 °N). The strong reduction in surface solar radiation (-3 W•m$^{-2}$) over North India is mainly due to the sulfate aerosols column connecting the boundary layer of the ASM region to the UTLS, with an additional contribution from the enhancement of sulfate aerosols in the ATAL (Fig. 3a). The increases in solar radiation over west India may be due to the low values of clouds (Fig. 7a) as mentioned in section 5.1

The anomalies in the temperature distribution induced by the enhancement of sulfate aerosol over the Indian region are shown in Figs.6c–d. The latitude-pressure cross section in Fig. 6c shows negative anomalies (-0.1±0.06 to -0.8±0.41 K) in the troposphere. Near the tropopause and in the lower stratosphere, temperature anomalies are positive (indicating warming of 0.1±0.06 to 0.6±0.25 K) extending from the Asian monsoon region (15 – 40 °N) to the North Pole. Figure 3a shows that this is the same altitude region where sulfate anomalies are positive (2 – 10 ng•m$^{-3}$), therefore causing an increased infra-red radiation absorption. Figure 6c depicts a warming up to ~1 K between 30 – 80 °N in the lower stratosphere, likely caused by the pole-ward transport of sulfate aerosol along a shallow branch of the BDC (see Fig 3b). Figure 6d shows the longitude-pressure cross sections of temperature anomalies, indicating a warming of 0.2±0.1 to 0.6±0.25 K near the tropopause and in the lower stratosphere and a cooling of -0.1±0.06 to -0.6 ± 0.25 K in the troposphere.

Figures 3b and 6d indicate that sulfate aerosols disperse east and westward from the monsoon anticyclone, leading to increased heating in that region (100 – 50 hPa). The negative anomaly in tropospheric temperature and subsidence (discussed in section 5.3) over north India produce a stabilization of the upper troposphere. The anomalies of Brunt-Väisälä frequency are positive (0.2 – 2 s$^{-1}$ × 10$^{-5}$) in the upper troposphere (250 – 70 hPa) over north India and the Tibetan plateau region 20 – 35 °N, 70 – 110 °E) (Fig.6e). This indicates that enhanced sulfate aerosols have increased the stability of the upper troposphere and produced anonymously low temperatures (Figs.6c–d) at these altitudes and over these regions. Upper tropospheric temperature and stability over the Tibetan plateau play an important role in the monsoon Hadley circulation and rainfall. The strong subsidence, upper tropospheric cooling over the Tibetan plateau and enhanced stability may likely produce deficit monsoon rainfall

(Wu and Zhang, 1998; Fadnavis et al., 2017c). However, a complete analysis of the impact of the enhanced surface aerosols on monsoon rainfall is beyond the scope of this study.

### 5.3 Cirrus Clouds

Cirrus clouds cover at least about 30 % of Earth's area over the year (Stubenrauch et al. 2013, Gasparini et al., 2018), occurring mainly between 400 – 100 hPa altitude. They play an important role in the Earth’s energy budget (Chen et al., 2000, Gasparini et al., 2016), in transport of water vapor into the stratosphere (Randel and Jensen, 2013), as well as in the atmospheric heat and energy cycle (Crueger and Stevens 2015; Hartmann et al., 2018). Cirrus clouds can form by either homogeneous nucleation by freezing of sulfate aerosols or by heterogeneous ice nucleation in presence of ice nuclei, most commonly dust (Ickes et al., 2015; Atkinson et al., 2013; Cziczo et al. 2016). Moreover, a large fraction of cirrus clouds have a liquid-origin history as the ice crystals were either nucleated at mixed-phase conditions and transported to lower temperatures or detrained from convective cloud tops (Krämer et al., 2016; Gasparini et al., 2018). All mentioned formation processes except heterogeneous nucleation of ice crystals below the homogeneous freezing temperature (i.e. at cirrus conditions) are simulated by our model simulations. However, heterogeneous freezing on dust and black carbon aerosols is included in mixed phase clouds (Lohmann and Hoose, 2009), for temperatures between freezing and -35°C.

Figure 7a shows a 5 – 10 % decrease of cirrus clouds over the North Indian region (20 – 35 °N) anomalies are negative, which coincides with the area of lofting of sulfate aerosols towards UTLS. This coincides with a significant decrease of ice crystal number concentration by 0.1 – 0.5 $cm^{-3}$ between 300 – 50 hPa (Fig. 7b–c). The increased upper tropospheric sulfate aerosol concentration leads to a temperature increase in the upper troposphere and lower stratosphere by about ~0.5 °C, and a cooling below (Fig. 6d). This decreases the upper tropospheric temperature gradient and increases the upper tropospheric (200 – 100 hPa) static stability (Brunt–Väisälä frequency) (over 80 – 120 °E) (Fig. 6e) and vertical velocity (23 – 40 °N) (Fig. 7d). A combination of decreased upper tropospheric updraft motion and increased temperatures decrease the likelihood of cirrus cloud formation in a similar way as for simulated responses to volcanic eruptions (Kuebbeler et al., 2012) or stratospheric sulfur geo-engineering (Visioni et al., 2018).

## 6. Summary and Conclusion

A ten-member ensemble ECHAM6–HAMMOZ model simulation for enhanced (by 48%) anthropogenic sulfate aerosols over South Asia was performed in order to understand the transport of sulfate aerosols in the monsoon anticyclone and their associated impacts on the global UTLS. The model simulations show transport of substantial amounts of anthropogenic sulfate aerosols from South Asia (75 – 95 °E, 8 – 35 °N) to the upper troposphere and lower stratosphere (UTLS) (anomalies ranging from 2 – 5 ng•$m^{-3}$) in the monsoon anticyclone and northern hemispheric lower stratosphere. This leads to substantial warming in the lower stratosphere (0.1±0.06 – 0.6±0.25 K) over the northern hemisphere and cooling in the troposphere over south Asia (-0.1±0.06 to -0.8±0.41 K). In addition, the net radiative forcing at the TOA is reduced over South Asia (-0.2 to -1.5 W•$m^{-2}$) and North India (23 – 30 °N, 75 – 85 °E) (~ -0.6 W•$m^{-2}$); the incoming solar radiation at the surface is also reduced over South Asia (-1 to -3 W•$m^{-2}$).

The RF at the TOA estimated for sulfate aerosols from the offline radiative transfer model is -0.3 to -1.3 W•m$^{-2}$ over South Asia, ~ -1.38 W•m$^{-2}$ over North India and ~ -0.1 W•m$^{-2}$ over mid-high latitudes. The magnitude of RF from ECHAM6–HAMMOZ simulations shows good agreement with the offline radiative transfer model. The minor differences may be due to implicit dynamical impacts in response to enhanced south Asian $SO_2$ emissions in ECHAM6–HAMMOZ, which are not represented in the offline model. We also estimate that the enhancement of sulfate aerosols in the UTLS (300– 50 hPa) produces a forcing of -0.012 to -0.02 W•m$^{-2}$ over North India.

Enhancement of South Asian anthropogenic sulfate aerosols leads to a decrease in cirrus clouds, a stronger subsidence, cooling of the upper troposphere over the northern regions of south Asia and over the Tibetan plateau. This enhances the stability (anomalies in Brunt Väisälä frequency 0.2 to 2 $s^{-1} \times 10^{-5}$) of the upper troposphere (250 – 70 hPa) of these regions. Upper tropospheric temperature and stability over the Tibetan plateau play an important role in impacting the monsoon Hadley circulation and rainfall. Strong subsidence, upper tropospheric cooling over the Tibetan plateau and enhanced stability are the features associated with deficit monsoon rainfall (Wu and Zhang, 1998; Fadnavis et al., 2017c). The link between these features and deficit monsoon rainfall should be addressed in future research.

It is important to note that an increase in surface emissions of $SO_2$ does not necessarily lead to a reduction in RF (as might be expected) but that regional enhancements of RF might occur in response to an inherent dynamical response (including changes in high cloud cover) to enhanced $SO_2$ emissions.

Atmos. Chem. Phys. Discuss., https://doi.org/10.5194/acp-2019-81
Manuscript under review for journal Atmos. Chem. Phys.
Discussion started: 1 March 2019


Data availability: OMI $SO_2$ data is obtained from https://disc.gsfc.nasa.gov/datasets/OMSO2e_V003/summary?keywords=aura, MISR data is available at https://giovanni.gsfc.nasa.gov/giovanni/, CALIPSO and CloudSat measurements are obtained from: http://www.cloudsat.cira.colostate.edu/data-products/. These satellite data sets are freely available.

Author contributions: S.F. designed the study and wrote the paper, G.K. analyzed the model simulations, M.R and A.R. performed offline radiative forcing computations. J.-Li provided CALIPSO data. B.G and A.L. helped with aerosols and cirrus cloud analysis. R.M. contributed to the writing and overall improvement of the manuscript.

*Acknowledgements*: Suvarna Fadnavis acknowledge Prof. Ravi Nanjundiah, Director of IITM, with gratitude for his encouragement during the course of this study. Authors thank a team high performance computing for supporting the model simulations.

## References

Atkinson, J. D., Murray, B. J., Woodhouse, M. T., Whale, T. F., et al.: The importance of feldspar for ice nucleation by mineral dust in mixed-phase clouds, Nature, 498, 355–358. https://doi.org/10.1038/nature12278, 2013.

Babu, S. S., Manoj, M. R., Moorthy, K. K., Gogoi, M. M., et al.: Trends in aerosol optical depth over Indian region: Potential causes and impact indicators, J. Geophys. Res., 118, 11,794–11,806, doi:10.1002/2013JD020507, 2013.

Bellouin, N., Rae, J., Jones, A., Johnson, C., Haywood, J., and Boucher, O.: Aerosol forcing in the Climate Model Intercomparison Project (CMIP5) simulations by HadGEM2-ES and the role of ammonium nitrate, J. Geophys. Res., 116, D20206, doi:10.1029/2011JD016074, 2011.

Crueger, T. and Stevens, B.: The effect of atmospheric radiative heating by clouds on the Madden-Julian Oscillation, J. Adv. Model. Earth Syst., 7, 854–864, doi:10.1002/2015MS000434, 2015.

Cziczo, D. J., Ladino, L., Boose, Y., Kanji, Z. A., Kupiszewski, P., et al.: Measurements of Ice Nucleating Particles and Ice Residuals, Meteorological Monographs, 58, 8.1-8.13. https://doi.org/10.1175/AMSMONOGRAPHS-D-16-0008.1, 2017.

Deng, M., Mace, G. G., Wang, Z., and Lawsan, R. P.: Evaluation of Several A-Train Ice Cloud Retrieval Products with In Situ Measurements Collected during the SPARTICUS Campaign, J. Appl. Meteorol. Clim., 52, 1014–1030, https://doi.org/10.1175/JAMCD-12-054.1, 2013.

Atmos. Chem. Phys. Discuss., https://doi.org/10.5194/acp-2019-81
Manuscript under review for journal Atmos. Chem. Phys.
Discussion started: 1 March 2019


DeMott, P. J., Prenni, A. J., Liu, X., Kreidenweis, S. M., Petters, M. D., et al.: Predicting global atmospheric ice nuclei distributions and their impacts on climate, P. Natl. Acad. Sci., 107, 11217–11222, https://doi.org/10.1073/pnas.0910818107, 2010.

Dumka, U. C., Moorthy, K. K., Kumar, R., Hegde, P., Sagar, R., et al.: Characteristics of aerosol black carbon mass concentration over a high altitude location in the Central Himalayas from multi-year measurements, Atmos., Res., 96, 510–521, 2010.

Edwards, J. M. and Slingo, A., Studies with a Flexible New Radiation Code. I: Choosing a Configuration for a Large-Scale Model, Quart. J. Roy. Metorol. Soc., 122, 689-719, http://dx.doi.org/10.1002/qj.49712253107, 1996.

Fadnavis, S., Roy, C., Chattopadhyay, R., Sioris, C. E., Rap, A., et al.: Transport of trace gases via eddy shedding from the Asian summer monsoon anticyclone and associated impacts on ozone heating rates, Atmos. Chem. Phys., 18, 11493–11506. https://doi.org/10.5194/acp-18-11493-2018, 2018.

Fadnavis, S., Kalita, G., Kumar, K. R., Gasparini, B., and Li, J.-L. F.: Potential impact of carbonaceous aerosol on the upper troposphere and lower stratosphere (UTLS) and precipitation during Asian summer monsoon in a global model simulation, Atmos. Chem. Phys., 17, 11637-11654, https://doi.org/10.5194/acp-17-11637-2017, 2017a.

Fadnavis, S., and Chattopadhyay, R.: Linkages of subtropical stratospheric intraseasonal intrusions with Indian summer monsoon deficit rainfall, J. Climate, 30, 5083–5095. https://doi.org/10.1175/JCLI-D-16-0463.1,2017b.

Fadnavis, S., Roy, C., Sabin, T. P., Ayantika, D. C., and Ashok, K.: Potential modulations of pre-monsoon aerosols during El Niño: impact on Indian summer monsoon, Clim. Dynam., 49, 2279–2290. https://doi.org/10.1007/s00382-016-3451-6., 2017c.

Fadnavis S., Dhomse, S., Ghude, S., Iyer, U., Buchunde, P., et al.: Ozone trends in the vertical structure of Upper Troposphere and Lower stratosphere over the Indian monsoon region, Int. J. Environ. Sci. Technol. 11, 529–542, doi 10.1007/s13762-013-0258-4,2014.

Fadnavis, S., Semeniuk, K., Pozzoli, L., Schultz, M. G., et al.: Transport of aerosols into the UTLS and their impact on the asian monsoon region as seen in a global model simulation, Atmos. Chem. Phys., 13, 8771–8786, https://doi.org/10.5194/acp-13-8771-2013, 2013.

Fadnavis, S. and Beig,G.: Seasonal variation of trend in temperature and ozone over the tropical stratosphere in the Northern Hemisphere, J. Atmos. Solar Terrestrial Phys., 68, 1952-1961, doi: 10.1016/j.jastp.2006.09.003, 2006.

Forster, P., et al., Changes in Atmospheric Constituents and in Radiative Forcing. In Climate Change 2007: The Physical Science Basis. Contribution of Working Group I to the Fourth Assessment Report of the Intergovernmental Panel on Climate Change [Solomon, S., D. Qin, M. Manning, Z. Chen, M. Marquis, K. B. Averyt, M. Tignor and H. L. Miller (eds.)] Cambridge University Press, Cambridge, United Kingdom and New York, NY, USA, 129-234., 2007.

Gasparini, B., Meyer, A., Neubauer,D., Münch, S., and Lohmann, U.: Cirrus Cloud Properties as Seen by the CALIPSO Satellite and ECHAM–HAM Global Climate Model, J. Climate, 31, 1983–2003, https://doi.org/10.1175/JCLI-D-16-0608.1, 2018.

Gasparini, B., and Lohmann, U.: Why cirrus cloud seeding cannot substantially cool the planet, J. Geophys. Res., 121, 4877–4893, https://doi.org/10.1002/2015JD024666, 2016.

Gu, Y., Liao, H., and Bian, J.: Summertime nitrate aerosol in the upper troposphere and lower stratosphere over the Ti-betan Plateau and the South Asian summer monsoon region, Atmos. Chem. Phys., 16, 6641-6663, https://doi.org/10.5194/acp-16-6641-2016, 2016.

Guo, L., Turner, A. G., and Highwood, E. J.: Local and remote impacts of aerosol species on indian summer monsoon rainfall in a GCM, J. Climate, 29, 6937–6955, https://doi.org/10.1175/JCLI-D-15-0728.1, 2016.

Hartmann, D. L., Gasparini, B., Berry, S. E., and Blossey, P. N.: The Life Cycle and Net Radiative Effect of Tropical Anvil Clouds, Journal of Advances in Modeling Earth Systems, 10, 3012–3029, https://doi.org/10.1029/2018MS001484, 2018.

Heckendorn, P., Weisenstein, D., Fueglistaler, S., Luo, B. P., Rozanov, E., Schraner, M., Peter, T.: The impact of geoengineering aerosols on stratospheric temperature and ozone, Environ. Res. Lett., 4, 045108, 1-12,https://doi.org/10.1088/1748-9326/4/4/045108, 2009.

Holben, B., Eck, T., Slutsker, I., Tanré, D., Buis, J., Setzer, A.,et al.: AERONET: Federated Instrument Network and Data Archive for Aerosol Characterization, Remote Sens. Environ., 66, 1–16, https://doi.org/10.1016/S0034- 4257(98)00031-5, 1998.

Ickes, L., Welti, A., Hoose, C. and Lohmann, U.: Classical nucleation theory of homogeneous freezing of water: thermodynamic and kinetic parameters, Phys. Chem. Chem. Phys.,17, 5514-5537, 10.1039/C4CP04184D, 2015.

Kahn, R., Banerjee P.D., McDonald D.: The sensitivity of multiangle imaging to natural mixtures of aerosols over ocean, J. Geophys. Res., 106,18219–18238,https://doi.org/10.1029/2000JD900497, 2001.

Kim, M. J., Yeh, S.-W. and Park, R. J.: Effects of sulfate aerosol forcing on East Asian summer monsoon for 1985–2010, Geophys. Res. Lett., 43, 1364–1372, doi:10.1002/2015GL067124, 2016.

Kinnison, D. E., Brasseur, G. P., Walters, S., Garcia, R. R., et al.: Sensitivity of chemical tracers to meteorological parameters in the MOZART-3 chemical transport model, J. Geophys. Res., 112, D20302, 1–24, https://doi.org/10.1029/2006JD007879, 2007.

Kokkola, H., Kühn, T., Laakso, A., Bergman, T., et al.: SALSA2.0: The sectional aerosol module of the aerosol–chemistry–climate model ECHAM6.3.0-HAM2.3-MOZ1.0, Geosci. Model Dev., 11, 3833–3863, https://doi.org/10.5194/gmd-11-3833-2018, 2018.

Krämer, M., Rolf, C., Luebke, A., Afchine, A., Spelten, N., et al.: A microphysics guide to cirrus clouds-Part 1: Cirrus types, Atmos. Chem. Phys., 16, 3463–3483, https://doi.org/10.5194/acp-16-3463-2016, 2016.

Kremser, S., Thomason, L. W., von Hobe, M., Hermann, M., et al: Stratospheric aerosol-Observations, processes and impact on climate, Rev. Geophys., 54, 278–335, https://doi.org/10.1002/2015RG000511, 2016.

Krotkov, N. A., McLinden, C. A., Li, C., Lamsal, L. N., et al.: Aura OMI observations of regional $SO_2$ and $NO_2$ pollution changes from 2005 to 2015, Atmos. Chem. Phys., 16, 4605–4629. https://doi.org/10.5194/acp-16-4605-2016, 2016.

Kuebbeler, M., Lohmann, U., and Feichter, J.: Effects of stratospheric sulfate aerosol geo-engineering on cirrus clouds, Geophys. Res. Lett., 39,L23803, 1–5. https://doi.org/10.1029/2012GL053797, 2012.

Lau, W. K. M., Yuan, C., and Li, Z.: Origin, Maintenance and Variability of the Asian Tropopause Aerosol Layer (ATAL): The Roles of Monsoon Dynamics, Sci. Rep., 8, 3960, 1–14. https://doi.org/10.1038/s41598-018-22267-z, 2018.

Atmos. Chem. Phys. Discuss., https://doi.org/10.5194/acp-2019-81
Manuscript under review for journal Atmos. Chem. Phys.
Discussion started: 1 March 2019


Lelieveld, J., Bourtsoukidis, E., Bruhl, C., Fischer, H., Fuchs, H., Harder, H., et al.: The South Asian monsoon pollution pump and purifier. Science, 361, 270–273, https://doi.org/10.1126/science.aar2501, 2018.

Levelt, P. F. et al.: The Ozone Monitoring Instrument, IEEE Trans. Geosci. Remote Sensing, 44, 1093–1101., 2006.

Li, J.-L.F., D. E. Waliser, W.-T. Chen, B. Guan, T. et al.: An observationally based evaluation of cloud ice water in CMIP3 and CMIP5 GCMs and contemporary reanalyses using contemporary satellite data, 117, D16105 J. Geophy. Res., doi:10.1029/2012JD017640, 2012.

Li, C., Joiner, J., Krotkov, N. A. and Bhartia, P. K.: A fast and sensitive new satellite $SO_2$ retrieval algorithm based on principal component analysis: Application to the ozone monitoring instrument, Geophys. Res. Lett., 40, 6314–6318. https://doi.org/10.1002/2013GL058134, 2013.

Li, C., McLinden, C., Fioletov, V., Krotkov, N., Carn, S., Joiner, J., et al.: India is overtaking China as the world's largest emitter of anthropogenic sulfur dioxide, Sci. Rep., 7, 14304, DOI:10.1038/s41598-017-14639-8, 2017.

Lohmann, U. and Ferrachat, S.: Impact of parametric uncertainties on the present-day climate and on the anthropogenic aerosol effect, Atmos. Chem. Phys., 10, 11373-11383, doi:10.5194/acp-10-11373-2010, 2010.

Lohmann, U. and Hoose, C.: Sensitivity studies of different aerosol indirect effects in mixed-phase clouds, Atmos. Chem. Phys., 9, 8917-8934, https://doi.org/10.5194/acp-9-8917-2009, 2009.

Manohar, G. K., Kahdalgaonkar, S. S., and Tinmaker, M. I. R.: Thunderstorm activity over India and the Indian southwest monsoon, J. Geophys. Res., , 104, 4169–4188. https://doi.org/10.1029/98JD02592, 1999.

Martonchik, J.V, Diner, D.J., Crean K. A. and Bull, M. A.: Regional aerosol retrieval results from MISR, IEEE Trans. Geosci. Remote Sens., 40, 1520–1531, 2002.

McPeters, R. D., Bhartia, P. K., Krueger, A. J. et al.,: Earth Probe Total Ozone Mapping Spectrometer (TOMS) Data Products User's Guide, https://www.academia.edu/28990900/Earth_Probe_Total_Ozone_Mapping_Spectrometer_TOMS_Data_Product_Users_Guide, 1996.

Myhre, G., Shindell, D., Bréon, F.-M., Collins, W., Fuglestvedt, J., et al.: Anthropogenic and Natural Radiative Forcing. Climate Change 2013: The Physical Science Basis. Contribution of Working Group I to the Fifth Assessment Report of the Intergovernmental Panel on Climate Change, 659–740, https://doi.org/10.1017/CBO9781107415324.018, 2013.

Neubauer, D., Lohmann, U. and Hoose, C. and Frontoso, M. G.: Impact of the representation of marine stratocumulus clouds on the anthropogenic aerosol effect, Atmos. Chem. Phys., 14, 11997–12022, doi:10.5194/acp-14-11997-2014, 2014.

Niemeier, U., and Schmidt, H.: Changing transport processes in the stratosphere by radiative heating of sulfate aerosols, Atmos. Chem. Phys., 17, 14871–14886. https://doi.org/10.5194/acp-17-14871-2017, 2017.

PadmaKumari, B., Londhe, A. L., Daniel, S., and Jadhav, D. B.: Observational evidence of solar dimming: Offsetting surface warming over India, Geophys. Res. Lett., 34, L21810, 1–5. https://doi.org/10.1029/2007GL031133, 2007.

Atmos. Chem. Phys. Discuss., https://doi.org/10.5194/acp-2019-81
Manuscript under review for journal Atmos. Chem. Phys.
Discussion started: 1 March 2019


Park, M., Randel, W. J., Emmons, L. K., and Livesey, N. J.: Transport pathways of carbon monoxide in the Asian summer monsoon diagnosed from Model of Ozone and Related Tracers (MOZART), J. Geophys. Res., 114, D08303, 2009.

Paul, S., Ghosh, S., Oglesby, R., Pathak, A., Chandrasekharan, A., and Ramsankaran, R.: Weakening of Indian Summer Monsoon Rainfall due to Changes in Land Use Land Cover, Sci. Rep., 6, 32177, 1–10, https://doi.org/10.1038/srep32177, 2016.

Pu, B., and Ginoux, P., How reliable are CMIP5 models in simulating dust optical depth? Atmos. Chem. Phys., 18, 12491-12510, https://doi.org/10.5194/acp-18-12491-2018, 12491–12510, 2018

Ramanathan, V., Chung, C., Kim, D., Bettge, T., Buja, L., Kiehl, J. T., et al.: Atmospheric brown clouds: Impacts on South Asian climate and hydrological cycle, P. Natl. Acad. Sci., 102, 5326–5333. https://doi.org/10.1073/pnas.0500656102, 2005.

Randel, W. and Jensen, E.: Physical processes in the tropical tropopause layer and their role in a changing climate, Nat. Geosci., 6, 169–176, https://doi.org/10.1038/ngeo1733, 2013.

Randel, W. J., and Park, M.: Deep convective influence on the Asian summer monsoon anticyclone and associated tracer variability observed with Atmospheric Infrared Sounder (AIRS). J. Geophys. Res. 111, D12314, 1–13, https://doi.org/10.1029/2005JD006490, 2006.

Rap, A., C. E. Scott, D. V. Spracklen, N. Bellouin, P. M. Forster, et al.: Natural aerosol direct and indirect radiative effects, Geophys. Res. Lett., 40,3297–3301, doi:10.1002/grl.50441, 2013.

Rolf, C., Vogel, B., Hoor, P., Afchine, A., Günther, G.,et al.: Water vapor increase in the lower stratosphere of the Northern Hemisphere due to the Asian monsoon anticyclone

Atmos. Chem. Phys. Discuss., https://doi.org/10.5194/acp-2019-81
Manuscript under review for journal Atmos. Chem. Phys.
Discussion started: 1 March 2019


observed during the TACTS/ESMVal campaigns, Atmos. Chem. Phys., 18, 2973-2983, https://doi.org/10.5194/acp-18-2973-2018, 2018.

Schultz, M. G., Stadtler, S., Schröder, S., Taraborrelli, D., et al.: The chemistry–climate model ECHAM6.3-HAM2.3-MOZ1.0, Geosci. Model Dev., 11, 1695-1723, https://doi.org/10.5194/gmd-11-1695-2018, 2018.

Smith, S. J., Van Aardenne, J., Klimont, Z., Andres, R. J., Volke, A., and Delgado Arias, S.: Anthropogenic sulfur dioxide emissions: 1850-2005, Atmos. Chem. Phys., 11, 1101–1116. https://doi.org/10.5194/acp-11-1101-2011, 2011.

Spada, M., Jorba, O., Pérez García-Pando, C., Janjic, Z, Baldasano, J. M.: Modeling and evaluation of the global sea-salt aerosol distribution: sensitivity to size-resolved and sea-surface temperature dependent emission schemes, Atmos. Chem. Phys., 13, 11735–11755. doi:10.5194/acp-13-11735-2013, 2013

Stier, P., Feichter, J., Kinne, S., Kloster, S., Vignati, E., Wilson, J., et al,.: The aerosol-climate model ECHAM5-HAM, Atmos. Chem. Phys., 5, 1125-1156, doi:10.5194/acp-5-1125-2005, 2005.

Storelvmo, T., Leirvik, T., Lohmann, U., Phillips, P. C. B., and Wild, M.: Disentangling greenhouse warming and aerosol cooling to reveal Earth's climate sensitivity, Nat. Geosci. 9, 286-289., http://doi.org/10.1038/NGEO2670, 2016.

Stubenrauch, C. J., Rossow, W. B., Kinne, S., Ackerman, S., Cesana, G., Chepfer, H., et al.: Assessment of Global Cloud datasets from Satellites: Project and Database initiated by the GEWEX Radiation Panel, Bull. Amer. Meteor. Soc., 1031-1048,. https://doi.org/10.1175/BAMS-D-12-00117.1, 2013.

Tegen, I., Neubauer, D., Ferrachat, S., Siegenthaler-Le Drian, C.,et al.: The aerosol-climate model ECHAM6.3-HAM2.3: Aerosol evaluation, Geosci. Model Dev. Discuss., 235, 1–54, https://doi.org/10.5194/gmd-2018-235, 2018.

Textor, C., Schulz, M., Guibert, S., Kinne, S., Balkanski, Y., et al.: Analysis and quantification of the diversities of aerosol life cycles within AeroCom, Atmos. Chem. Phys., 6, 1777–1813,https://doi.org/10.5194/acp-6-1777-2006, 2006.

Thomason, L. W. and Vernier, J.-P.: Improved SAGE II cloud/aerosol categorization and observations of the Asian tropopause aerosol layer: 1989–2005, Atmos. Chem. Phys., 13, 4605-4616, https://doi.org/10.5194/acp-13-4605-2013, 2013.

Verma, S., Boucher, O., Shekar Reddy, M., Upadhyaya, H. C., et al. : Tropospheric distribution of sulfate aerosols mass and number concentration during INDOEX-IFP and its transport over the Indian Ocean: A GCM study, Atmos. Chem. Phys., 12, 6185–6196. https://doi.org/10.5194/acp-12-6185-2012, 2012.

Vernier, J. P., Fairlie, T. D., Deshler, T., Venkat Ratnam, M., Gadhavi, et al.: BATAL: The balloon measurement campaigns of the Asian tropopause aerosol layer, Bull. Amer. Meteor. Soc., 99, 955–973. https://doi.org/10.1175/BAMS-D-17-0014.1, 2018.

Vernier, J. P., Fairlie, T. D., Natarajan, M., Wienhold, F. G., Bian, J., et al.: Increase in upper tropospheric and lower stratospheric aerosol levels and its potential connection with Asian pollution, J. Geophys. Res., 120, 1608–1619. https://doi.org/10.1002/2014JD022372, 2015.

Vernier, J. P., Thomason, L. W., and Kar, J.: CALIPSO detection of an Asian tropopause aerosol layer, Geophys. Res. Lett., 38, L07804, 1–6. https://doi.org/10.1029/2010GL046614, 2011.

Vignati, E., Wilson,J., and Stier,P.: An efficient size-resolved aerosol microphysics module for large-scale aerosol transport models, J. Geophys. Res., 109, D22202, doi:10.1029/2003JD004485, 2004.

Vinoj, V., Rasch, P. J., Wang, H., Yoon, J.-H., Ma, P.-L., Landu, K., and Singh, B.: Short-term modulation of Indian summer monsoon rainfall by West Asian dust, Nat. Geosci., 7, 308–313, https://doi.org/10.1038/ngeo2107, 2014.

Visioni, D., Pitari, G., di Genova, G., Tilmes, S., and Cionni, I.: Upper tropospheric ice sensitivity to sulfate geoengineering, Atmos. Chem. Phys., 18, 14867-14887, https://doi.org/10.5194/acp-18-14867-2018, 2018.

Vogel, B., Müller, R., Günther, G., Spang, R., Hanumanthu, S., et al.: Lagrangian simulations of the transport of young air masses to the top of the Asian monsoon anticyclone and into the tropical pipe, Atmos. Chem. Phys. Discuss., https://doi.org/10.5194/acp-2018-724, in review, 2018.

Vogel, B., Günther, G., Müller, R., Grooß, J.-U., Afchine, A., et al.: Long-range transport pathways of tropospheric source gases originating in Asia into the northern lower stratosphere during the Asian monsoon season 2012, Atmos. Chem. Phys., 16, 15301-15325, https://doi.org/10.5194/acp-16-15301-2016, 2016

Vogel, B., Günther, G., Müller, R., Grooß, J.-U., Hoor, P., Krämer, M., et al.: Fast transport from Southeast Asia boundary layer sources to northern Europe: rapid uplift in typhoons and eastward eddy shedding of the Asian monsoon anticyclone, Atmos. Chem. Phys., 14, 12745-12762, https://doi.org/10.5194/acp-14-12745-2014, 2014.

Atmos. Chem. Phys. Discuss., https://doi.org/10.5194/acp-2019-81
Manuscript under review for journal Atmos. Chem. Phys.
Discussion started: 1 March 2019


Winker, D., Pelon, J., Coakley, J., Ackerman, S., Charlson, R., et al.: The CALIPSO MISSION A Global 3D View of Aerosols and Clouds. Bull. Amer. Met. Soc.,91, 1211-1229, doi: http://dx.doi.org/10.1175/2010bams3009.1, 2010.

Wu, G. X. and Zhang, Y. S.: Tibetan Plateau forcing and the timing of the monsoon onset over South Asia and the South China Sea, Monthly Weather Rev., 126, 913–927, *https://doi.org/10.1175/1520-0493(1998)126<0913:TPFATT>2.0.CO;2*,1998.

Yu, P., Toon, O. B., Neely,R. R., Martinsson, B. G. and Brenninkmeijer C. A. M.: Composition and physical properties of the Asian Tropopause Aerosol Layer and the North American Tropospheric Aerosol Layer. Geophys. Res. Lett., 42, 2540–2546. doi: 10.1002/2015GL063181, 2015.

Yu, P., Murphy, D. M., Portmann, R. W., Toon, O. B., Froyd, K. D., Rollins, A. W., et al.: Radiative Forcing from anthropogenic sulfur and organic emissions Reaching the Stratosphere, Geophys. Res. Lett., 43, 9361–9367, https://doi.org/10.1002/2016GL070153, 2016.

Yu, P., Rosenlof, K. H., Liu, S., Telg, H., Thornberry, T. D., Rollins, A. W., et al.: Efficient transport of tropospheric aerosol into the stratosphere via the Asian summer monsoon anticyclone. P. Natl. Acad. Sci., 114, 6972–6977. https://doi.org/10.1073/pnas.1701170114, 2017.

Zhang, J, Christopher, S,A.: Longwave radiative forcing of Saharan dust aerosols estimated from MODIS MISR and CERES observations on Terra, Geophys. Res. Lett., 30, 2188.doi:10.1 029/2003GL018479, 2003.

Zhang, K., O'Donnell, D., Kazil, J., Stier, P., Kinne, S., et al.: The global aerosol-climate model ECHAM-HAM, Version 2: Sensitivity to improvements in process representations, Atmos. Chem. Phys., 12, 8911-8949, https://doi.org/10.5194/acp-12-8911-2012, 2012.

Atmos. Chem. Phys. Discuss., https://doi.org/10.5194/acp-2019-81
Manuscript under review for journal Atmos. Chem. Phys.
Discussion started: 1 March 2019


Table 1: Details of model simulations performed.

| Sr. No | Experiment description | Name of experiment | SST and Sea Ice | Initial condition of the simulation | Analysis is performed for period |
|---|---|---|---|---|---|
| 1. | Control simulation | CTRL | Varying SST and Sea ice | 1 – 10 January 2010 | June – September 2011 |
| 2. | The anthropogenic emissions of $SO_2$ over India (8 – 40 °N; 70 – 95 °E) are increased by 48 %. | Ind48 | Varying SST and Sea ice | 1 – 10 January 2010 | June – September 2011 |

Atmos. Chem. Phys. Discuss., https://doi.org/10.5194/acp-2019-81
Manuscript under review for journal Atmos. Chem. Phys.
Discussion started: 1 March 2019

Atmospheric Chemistry and Physics
Discussions

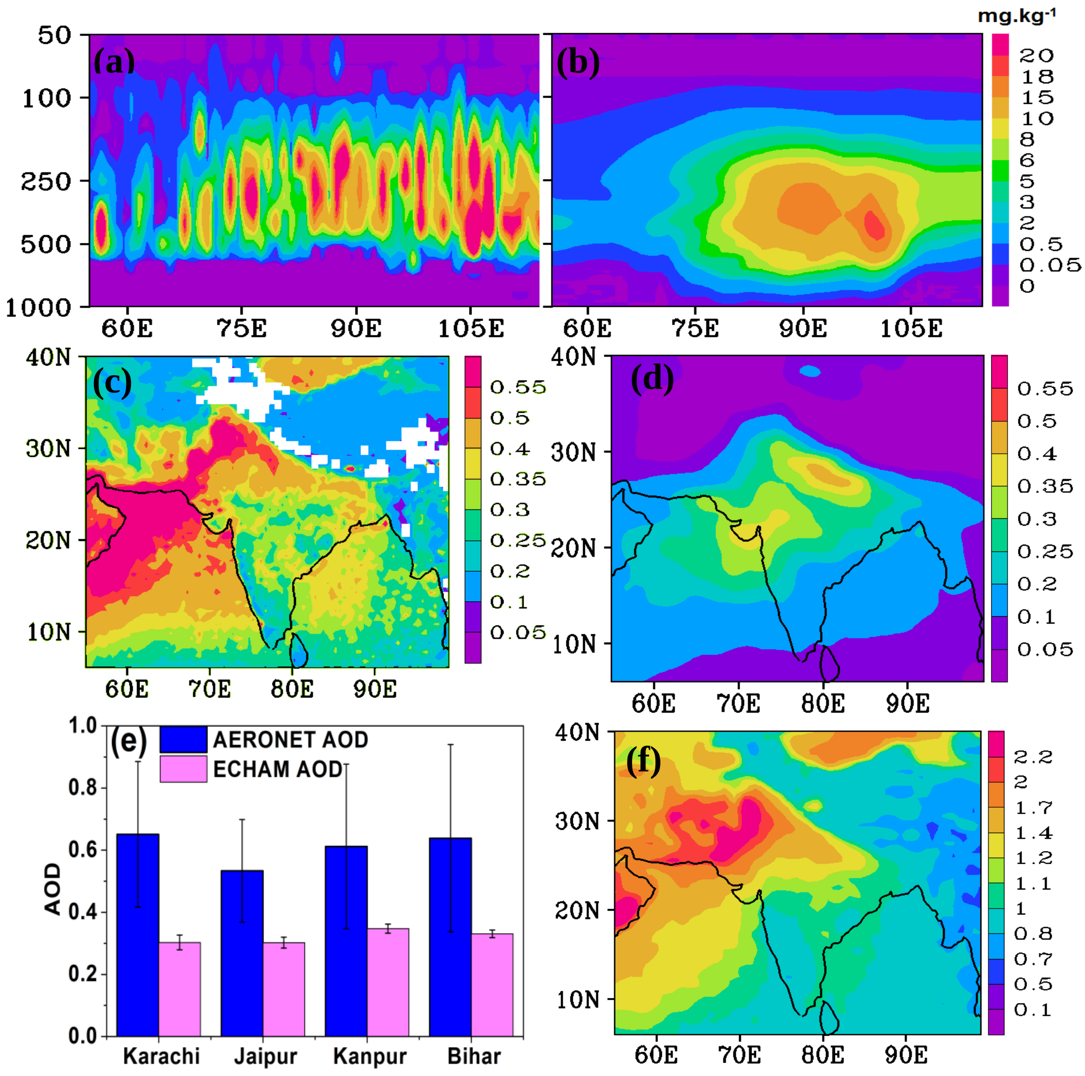


Figure 1 : Seasonal mean distribution of (a) cloud ice mass mixing ratio (mg•kg$^{-1}$) from CloudSat and CALIPSO combined 2C–ICE L3 for the years 2007 – 2010, (b) cloud ice mass mixing ratio (mg•kg$^{-1}$) averaged for 20 – 40 °N from CTRL simulations. Distribution of seasonal mean (June-September) Aerosol Optical Depth (AOD) from (c) MISR for the period 2000 – 2016, (d) AOD from ECHAM6–HAMMOZ CTRL simulations, (e) comparison of AOD from the model simulations and AERONET (2006 – 2016) at the stations: Bihar, Jaipur, Kanpur, and Karachi, (f) TOMS AI for 1997 – 2005. The dashed box in Fig. (c) indicates the region (70 – 95 °E, 8 – 35 °N) of $SO_2$ emission enhancement by 48 %.

Atmos. Chem. Phys. Discuss., https://doi.org/10.5194/acp-2019-81
Manuscript under review for journal Atmos. Chem. Phys.
Discussion started: 1 March 2019

Atmospheric Chemistry and Physics
Discussions
Open Access

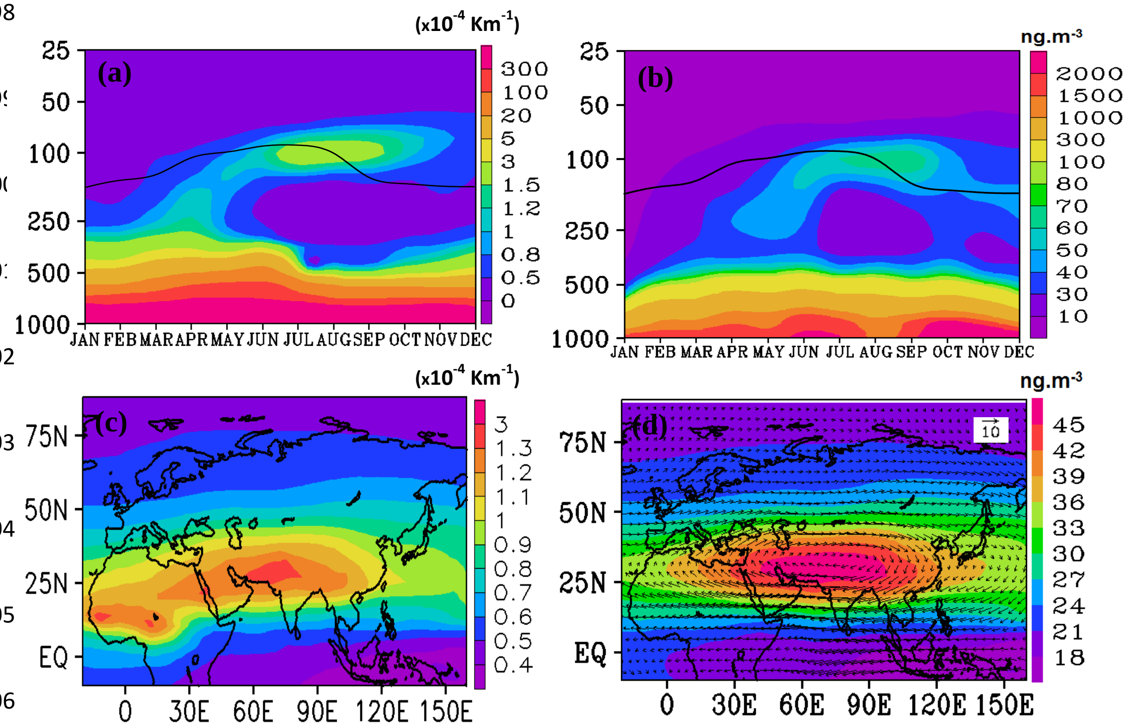


Figure 2 : Monthly vertical variation of (a) extinction (km$^{-1}$× 10$^{-4}$) averaged for 80 – 95 °E, 25 – 40 °N, (b) sulfate aerosols (ng•m$^{-3}$) averaged over 75 – 95 °E, 25 – 40 °N, (c) distribution aerosol extinction (km$^{-1}$ × 10$^{-4}$) at 100hPa averaged for the monsoon (JJAS) season, (d) Distribution of sulfate aerosol at 100 hPa averaged for the monsoon (JJAS) season. Wind vectors in (d) indicate extent of the anticyclone. (a)–(d) are obtained from CTRL simulations.

Atmos. Chem. Phys. Discuss., https://doi.org/10.5194/acp-2019-81
Manuscript under review for journal Atmos. Chem. Phys.
Discussion started: 1 March 2019


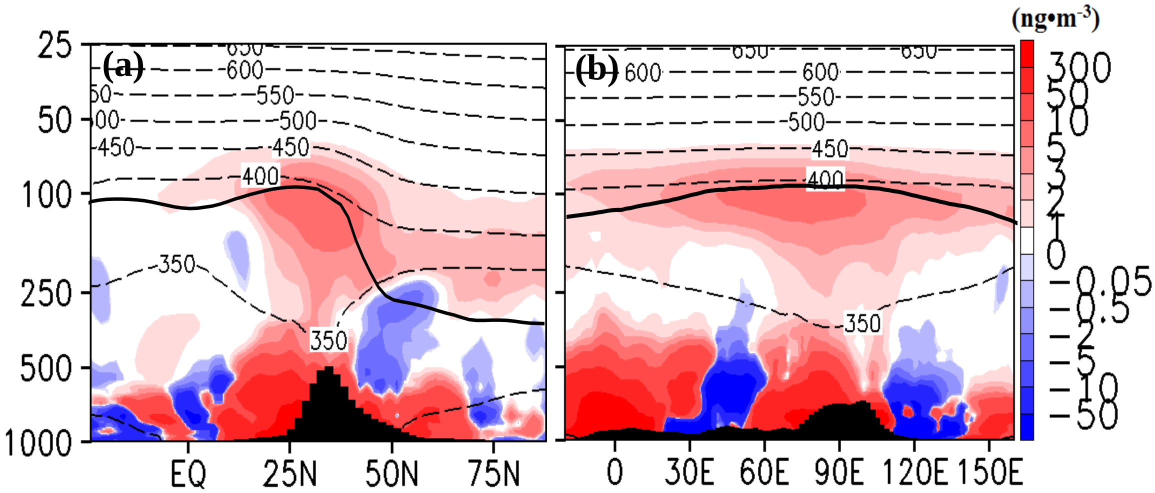


Figure 3: Distribution of anomalies of sulfate aerosols (ng•m$^{-3}$) averaged for the monsoon season (a) latitude–pressure cross sections averaged over 75 – 95 °E (b) longitude–pressure cross section averaged over 15 – 35 °N. The thick black line represents the tropopause height and the dashed lines represent the potential temperature (θ).

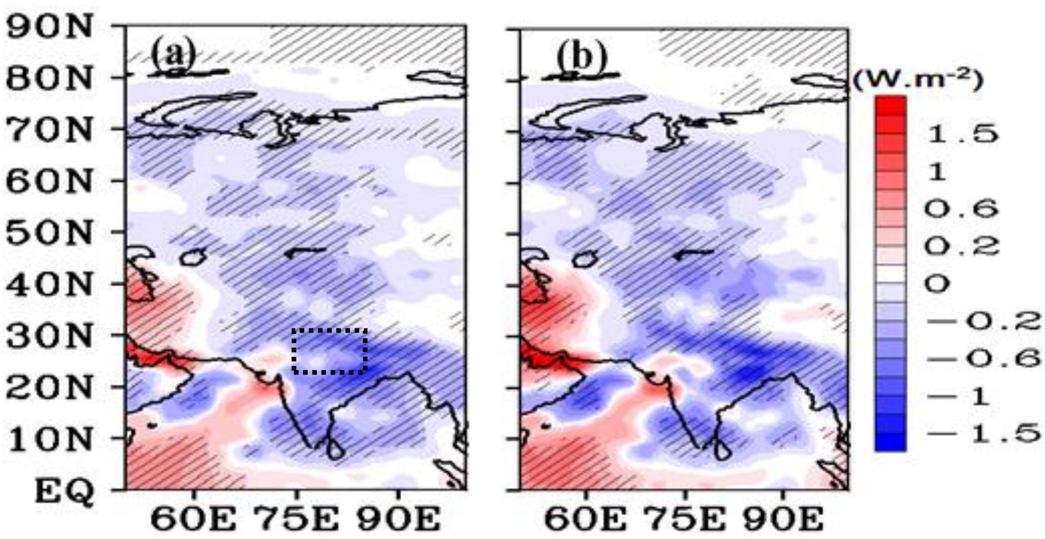


Figure 4: Clear sky direct net radiative forcing (W•m$^{-2}$) due to enhanced sulfate aerosols simulated by ECHAM6–HAMMOZ (a) at the top of the atmosphere, and (b) at the surface. North India (23 – 30 °N, 75 – 85 °E) is indicated by a box. The black hatched lines indicate the 90 % significance level.

Atmos. Chem. Phys. Discuss., https://doi.org/10.5194/acp-2019-81
Manuscript under review for journal Atmos. Chem. Phys.
Discussion started: 1 March 2019


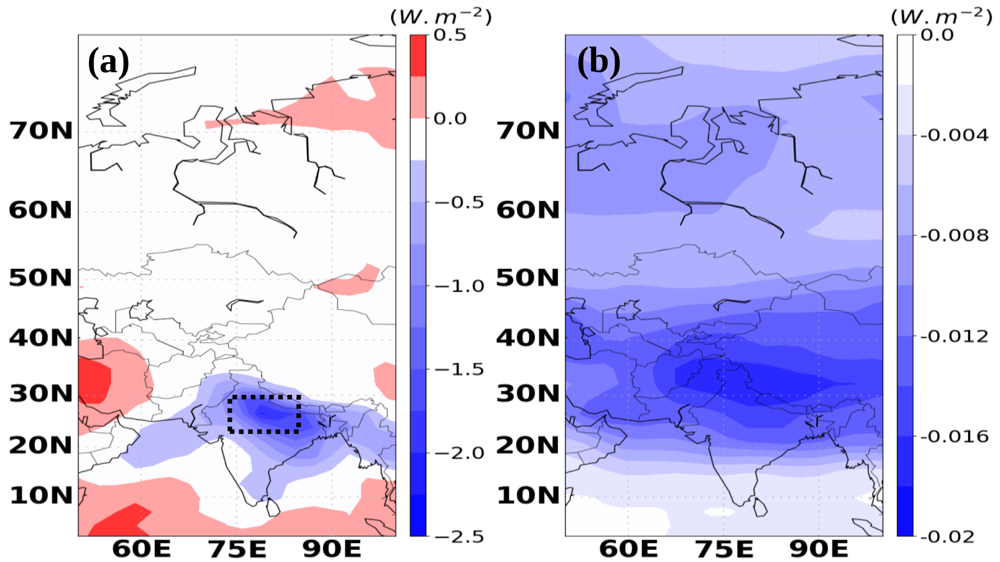


Figure 5: Clear sky TOA direct net radiative forcing (W•m$^{-2}$) simulated by our offline experiments due to (a) all atmosphere and (b) UTLS–only enhanced sulfate aerosol loadings. North India (23 – 30 °N, 75 – 85 °E) is indicated by a box.

Atmos. Chem. Phys. Discuss., https://doi.org/10.5194/acp-2019-81
Manuscript under review for journal Atmos. Chem. Phys.
Discussion started: 1 March 2019


Atmospheric Chemistry and Physics
Discussions
Open Access

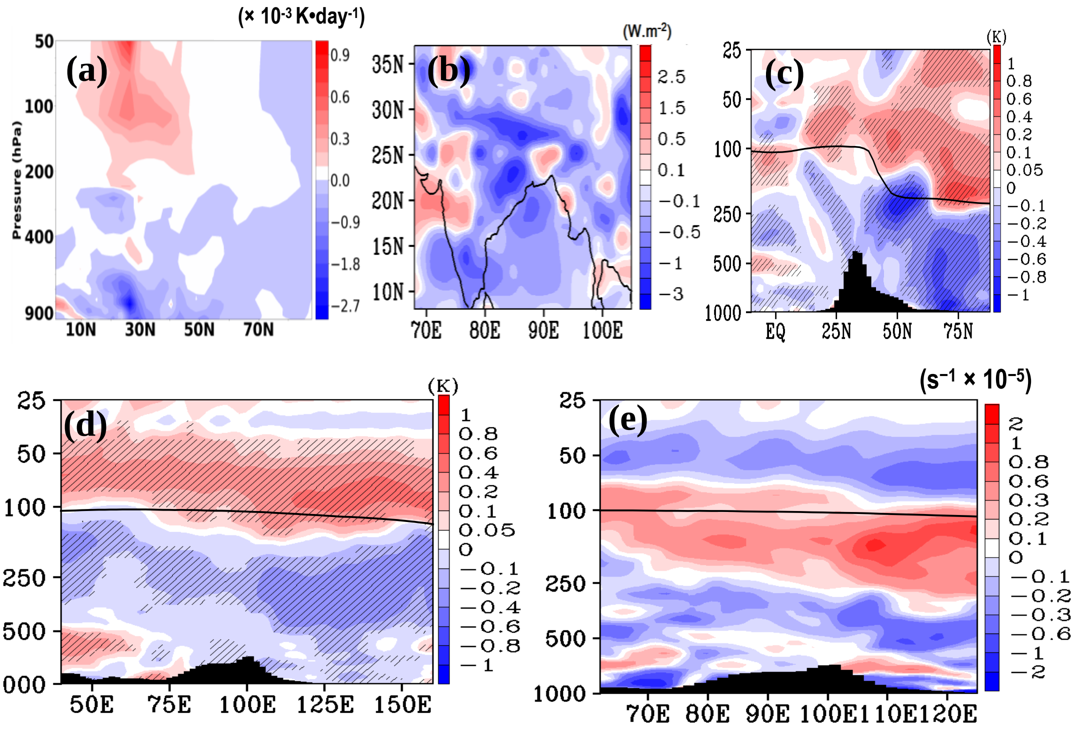


Figure 6: Distribution of anomalies in (a) Net sulfate heating rate ($\times 10^{-3}$ K•day$^{-1}$) (b) net solar radiations (W•m$^{-2}$) at the surface. Distribution of anomalies in temperature (K), (c) latitude-pressure cross section averaged over 80 – 90 °E, (d) Longitude pressure cross section averaged over 20 – 30 °N. In (c–e) the black hatched lines indicate the 90 % significance level and thick black line indicates the tropopause. (e) Brunt–Väisälä frequency (s$^{-1}$ $\times$ 10$^{-5}$) averaged over 25 – 40 °N.

Atmos. Chem. Phys. Discuss., https://doi.org/10.5194/acp-2019-81
Manuscript under review for journal Atmos. Chem. Phys.
Discussion started: 1 March 2019


Atmospheric Chemistry and Physics
Open Access
Discussions

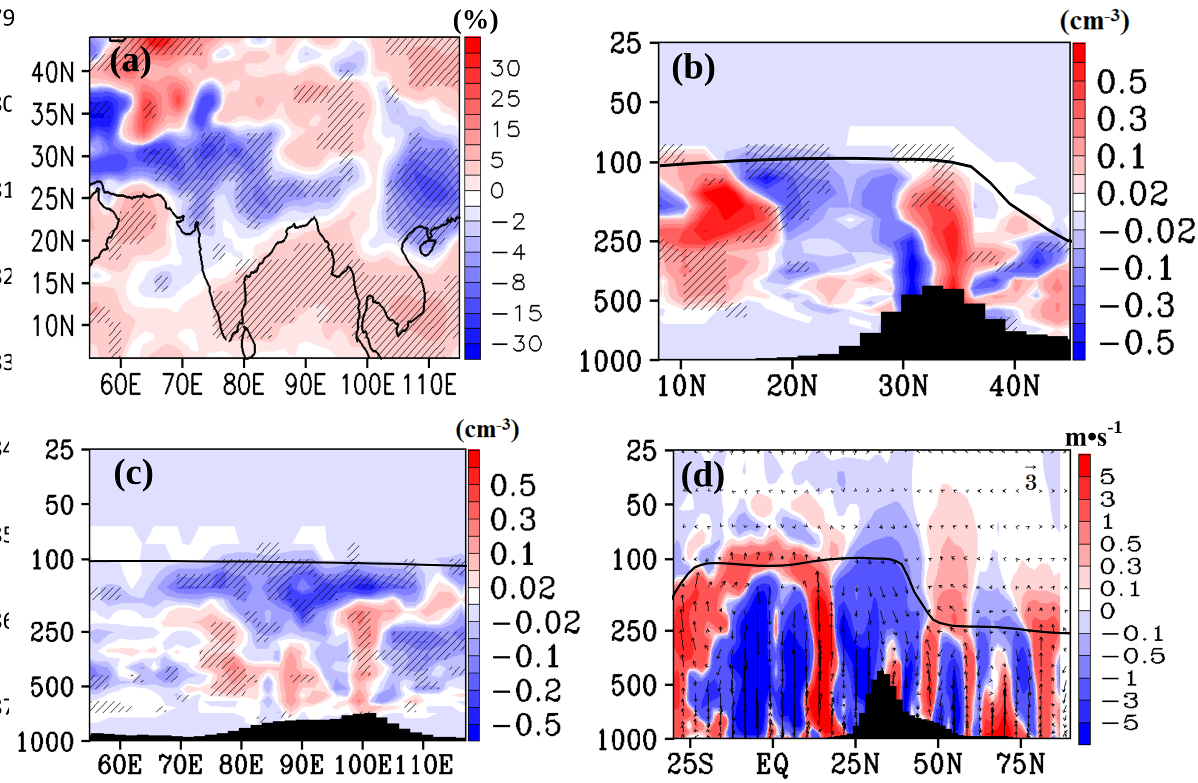


Figure 7: Distribution of anomaly in (a) high cloud (%), (b) Latitude-press cross section of anomaly in ICNC ($cm^{-3}$) averaged over 80 – 90 °E, (c) Longitude cross section of anomaly in ICNC ($cm^{-3}$) averaged over 20 – 30 °N. The black hatched line in Fig. (a–c) indicates 90 % significance level, (d) Anomaly in vertical velocity ($m•s^{-1}$). Vertical velocity is scaled by 1000. In (b)–(d) thick black line indicates the tropopause.